Article

One-Pot Synthesis of Bright Blue Luminescent N-Doped GQDs: Optical Properties and Cell Imaging

Huaidong Wang [1], Chong Qi [1], Ailing Yang [1,*], Xiaoxu Wang [2] and Jie Xu [2]

[1] College of Physics & Optoelectronic Engineering, Ocean University of China, Qingdao 266100, China; wanghuai-dong@stu.ouc.edu.cn (H.W.); qichong@stu.ouc.edu.cn (C.Q.)
[2] College of Food Science & Engineering, Ocean University of China, Qingdao 266003, China; wangxx0416@163.com (X.W.); xujie9@ouc.edu.cn (J.X.)
* Correspondence: ailingy@ouc.edu.cn

Abstract: High fluorescent graphene quantum dots (GQDs) are promising in bioimaging and opto-electronics. In this paper, bright blue fluorescent N-doped GQDs were synthesized using a ultrasonic-assisted hydrothermal method. The morphology, structure, surface chemistry, optical properties, and stability subject to photo-bleaching, temperature, pH and preservation period for the N-GQDs were investigated in detail using various microscopy and spectroscopy techniques. The results showed that the N-GQDs possessed an average size of 2.65 nm, 3.57% N doping, and up to 54% quantum yield (QY). The photoluminescence (PL) spectra of the N-GQDs are excitation dependent when excited in the range of 300–370 nm and excitation independent in the range of 380–500 nm for the core and surface states emission. The N-GQDs showed excellent photo-bleaching resistance and superior photo-stability. At room temperature and in the pH range of 3–8, the fluorescence of the N-GQDs was almost invariable. The N-GQDs can be stably preserved for at least 40 days. The average decay lifetime of the N-GQDs was 2.653 ns, and the radiative and nonradiative decay rate constants were calculated to be 2.04×10^8 s^{-1} and 1.73×10^8 s^{-1}, respectively. The PL mechanism was qualitatively explained. The N-GQDs was used for cell imaging, and it showed good results, implying great potential applications for bioimaging or biomarking.

Keywords: ultrasonic-assisted hydrothermal; nitrogen doped graphene quantum dots; optical properties; photo-stability; cell imaging

1. Introduction

Graphene (Gr) and its derivative graphene oxide (GO) have been a hot research direction in materials science in recent years [1–7]; however, applications of Gr in the fields of bioimaging and optoelectronics have been limited, because Gr is a zero-band-gap semiconductor and a non-fluorescent substance. Graphene quantum dots (GQDs) are small sheets of Gr with lateral size of less than 10 nm, with oxygen-containing groups at the edges. As a result of the quantum confinement effect and the lateral effect, GQDs are fluorescent matter. In addition to this, GQDs possess other outstanding advantages, such as their being green, nontoxic, chemically inert, possessing good aqueous solubility and excellent biocompatibility, and lending themselves to easy modification, rendering GQDs as one of the most promising fluorescent nanomaterials, superior to conventional fluorescent organic dyes and luminescent inorganic quantum dots, with extensive potential applications in bioimaging [8–10], as drug carriers [11], and in disease diagnosis [12], optical sensors [13–15], solar cells [16–18], light emitting diodes [19], and photocatalysts [20]. Several methods have been developed for the fabrication of GQDs. Generally, these approaches can be classified into two types: top-down and bottom-up. Top-down methods are mainly based on cutting the large carbon materials into nanoparticles (NPs), such as through the chemical exfoliation of graphite NPs [21] and the hydrothermal cutting of oxidized graphene sheets [22]. Top-down methods may produce some toxic products [23] that are difficult to completely

remove in post-treatment procedures, thus leading to environmental pollution, causing health hazards to humans, and also limiting their widespread use. Bottom-up approaches use small molecules containing C, H, and O as precursors, via solid phase pyrolysis or hydrothermal condensation, to obtain GQDs [24,25].

Nitrogen-doped GQDs (N-GQDs) may improve the fluorescent quantum yield (QY) by adjusting the photoluminescence (PL) range. This enhances biocompatibility, and therefore, the properties of N-GQDs have attracted a significant amount of research interest [26]. The direct pyrolysis of small molecules in solid phase [27–29] and via the hydrothermal route [12,30,31] has been used to prepare N-GQDs. The direct pyrolysis of small molecules in solid phase to obtain N-GQDs is simple and quick, but small molecules are easily over-carbonized, and large particles can readily be produced, leading to a product with a wide size distribution and complex post-treatment procedures. The negative effects the direct pyrolytic method described above restrict its widespread use in the preparation of N-GQDs. The hydrothermal route seems to be the key to solving the problems inherent in the direct pyrolysis of small molecules in solid phase [32]. The ultrasonic hydrothermal method has distinct advantages with respect to maintaining homogeneous reaction conditions to prevent the N-GQDs from agglomerating, as well as providing a shorter reaction time, milder reaction conditions, lower energy consumption, better stability, and good reproducibility. Thus, in this paper, an ultrasonic hydrothermal method was used to synthesize N-GQDs in one step, with citric acid (CA) as a precursor and L-glutamic (L-Glu) for N doping and as a passivant. Compared to the two-step approach (first fabrication of GQDs, then amino-modification), the one-step strategy is easier and saves time; more importantly, the L-Glu functionalized GQDs have the benefit of decreasing the surface defects of GQDs, thus enhancing the QY and stability, and improving biocompatibility. The as-prepared N-GQDs were characterized in detail and used for cell imaging. The results indicated that the N-GQDs possessed excellent photo-physical properties and were effective in BV2 cell imaging. In this regard, this new strategy overcomes the limitations of existing N-GQDs, by reducing the surface defects, increasing the QY and stability, and improving biocompatibility.

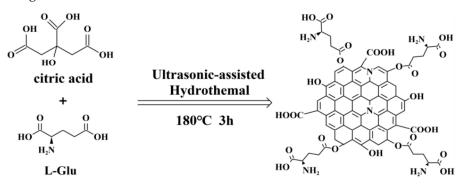## 2. Experimental Section

2.1. Materials and Characterization

L-Glu, CA and Rhodamine B reagents were all of analytical grade and were purchased from Aladdin Reagent Co., Ltd. (Shanghai, China). Ultrapure water (18.2 MΩ·cm) was used as a solvent. Propidium iodide (95%), Dulbecco's modified Eagle medium (DMEM) and fetal bovine serum (FBS) were bought from Gibco (Gaithersburg, MD, USA). Penicillin and streptomycin sulfate were purchased from Invitrogen.

An YZUR-100 (Shanghai Yan Zheng, Shanghai, China) ultrasonic hydrothermal reactor (220 V) was used to synthesize N-GQDs; the ultrasonic power could be adjusted within 250 W, and the stirring speed was 200 rad/min; the pressure in the cavity was controlled between 0.84–0.88 MPa. The ultraviolet-visible (UV-Vis) absorption spectra were determined using a UH5300 spectrophotometer (Hitachi, Japan) at room temperature. PL spectra were measured using a FluoraMAX-4 fluorescent spectrometer (Horiba JY, Edison, NJ, USA) with excitation/emission slit width of 2/3 nm. The crystalline structure of N-GQD solid powder was characterized using an X-ray diffractometer (XRD, Bruker D8 ADVANCE, BRUKER AXS, Germany) with Cu-Kα radiation (λ = 1.5406 Å). A high-resolution transmission electron microscope (HRTEM, Tecnai G2 F30 Hillsboro, OR, USA) was used to observe the morphology and lattice of the N-GQDs prepared on an ultra-thin carbon film. The size distribution of the N-GQDs was analyzed with Image J software. By coating the diluted N-GQDs on freshly dissociated mica, the surface morphology and thickness of N-GQDs were characterized using an atomic force microscope (AFM, Seiko-SPA400, Tokyo, Japan) with ScanAsys atomic imaging optimization technology. Fourier transform infrared (FTIR) spectroscopy was employed using a Nicolet iN10 FTIR spectrometer (Thermo Fisher Scientific, Waltham, MA, USA) with a resolution of 4 cm^{-1} from 4000 to 500 cm^{-1}. The

test sample was prepared by grinding, mixing then pressing of 2 mg powder of N-GQDs and 100 mg KBr powder. X-ray Photoelectron Spectroscopy (XPS) with a multifunctional imaging electron spectrometer (Thermo ESCALAB 250XI, America, with a radiation source Al Kα-1486.6 eV) was used to analyze the elemental compositions and chemical bonds of the obtained N-GQDs. The fluorescence lifetime of the N-GQDs was measured using the time-correlated single photon counting (TCSPC) technique, an Edinburgh F900 time-resolved fluorescence spectrometer (FLS-980, Edinburgh, UK) with an LED excitation source (370 nm), and an electrically cooled red sensitive R928P photon-counting photomultiplier tube detector to obtain the fluorescence lifetime, with a monitor emission wavelength of 440 nm. An incubator (Thermo Fisher Scientific, Waltham, MA, USA) was employed to culture BV2 cells. Cell imaging was performed using a confocal laser scanning microscope (LSM, Nikon A1R HD25, Tokyo, Japan) with three semiconductor lasers (405, 488, and 532 nm).

2.2. Preparation of N-GQDs

The ultrasonic-assisted method was used to fabricate the N-GQDs as shown in Scheme 1. The natural organic acid CA provided the carbon source, and the natural amino acid L-Glu supplied the amino group and part of the carbon source to achieve nitrogen doping. In the fabrication process, the reaction temperature (180 °C) was higher than the boiling point of CA (160 °C), but lower than that of the L-Glu (225 °C); therefore, CA was pyrolyzed, dehydrated and condensed to form GQDs. GQDs possess COOH and OH at the surfaces and edges; through the dehydration reaction, L-GLu was linked to GQDs, so the GQDs were functionalized by L-Glu in a single step, which is of great benefit for decreasing the surface defects on GQDs, thus enhancing the QY [33,34]. The amino groups in GQDs make them useful in the field of biomedicine [35]. The synthesis was optimized step by step (the experimental process is shown in the Supporting Information, see Figure S1 and Table S1). Typically, 3.6 g CA and 1.8 g L-Glu were dispersed into 30 mL deionized water; the solution was heated up to 180 °C in the ultrasonic hydrothermal reactor and kept at a constant temperature for 3 h; then the solution was cooled down to room temperature. By filtrating three times (filter with 0.22 μm hole) and dialysis (1000 D) for 18 h, a pure N-GQD solution was obtained. After freeze drying, solid-phase N-GQDs were obtained and stored in a refrigerator at 4 °C for later use.

Scheme 1. Schematic diagram of the formation of N-GQDs by ultrasonic-assisted hydrothermal method.

3. Results and Discussion

3.1. Morphology and Structure of the N-GQDs

The morphology and structure of the N-GQDs were characterized in detail using TEM, HRTEM, AFM and XRD. Figure 1 presents the experimental results; TEM (Figure 1A) shows that the N-GQDs have a good dispersity, with most N-GQDs being circular nanosheets; the statistical calculation for more than 100 N-GQDs indicated that the average diameter of the N-GQDs was about 2.65 nm (Figure 1B); the clear and regular lattice fringes in the HRTEM image (Figure 1C) indicate that the interplanar spacing of the N-GQDs was 0.213 nm, which is equivalent to graphite carbon [36]; AFM images (Figure 1D,E) indicate that the heights

of the N-GQDs were in the range of 1.5–4.5 nm, implying that the N-GQDs contained 4–12 layers of graphene [37]; the XRD pattern of the N-GQDs indicates a wide diffraction peak at $2\theta = 21.06°$, corresponding to the (002) crystal facet of graphene [38]. According to the Bragg equation $2dSin\theta = \lambda$ [39], the layer spacing was about d = 0.36 nm, which is larger than that of graphite (0.335 nm) [40]; the main reasons for this are the nitrogen doping of the GQDs and the oxygen-containing functional groups at the edges of the GQDs [41].
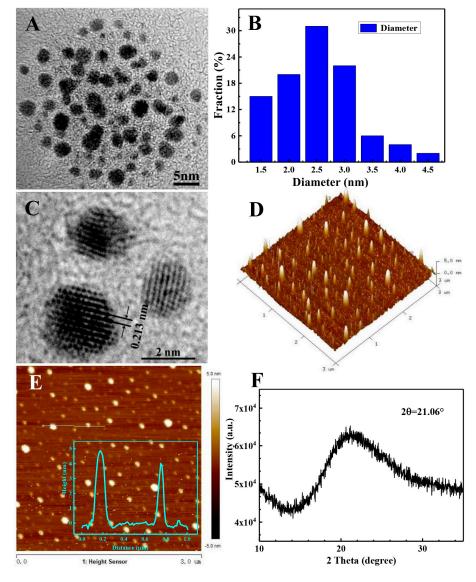

Figure 1. (**A**) TEM, (**B**) size distribution, (**C**) HRTEM, (**D**,**E**) AFM, and (**F**) XRD pattern of the N-GQDs.

3.2. Surface Chemistry of the N-GQDs

The surface chemical architectures of the N-GQDs were detected using FTIR (Figure 2) and XPS (Figure 3). For comparison, the FTIR spectra of pure CA and L-Glu were also measured (Figure 2a,b). The FTIR spectrum of CA shows O–H stretching (3490–3280 cm^{-1}), C=O stretching (1750 and 1710 cm^{-1}), –CH$_2$– scissor vibration (1430 cm^{-1}), –CH$_2$– oscillation out of plane (1390 cm^{-1}), in-plane deformation vibration of C–OH bond (1180–1290 cm^{-1} and 1310–1360 cm^{-1}), twisting vibration of –CH$_2$– (1220–1240 cm^{-1}), C–O stretching (1080–1140 cm^{-1}) and C–C stretching (1050 cm^{-1}) peaks (Figure 2a) [42,43]. The FTIR of L-Glu (Figure 2b) exhibits O–H and N–H stretching (2780–3600 cm^{-1}), –C–H stretching (2650–2740 cm^{-1}), carboxylic acid of C=O stretching (1740 and 1640 cm^{-1}), N–H out-of-plane bending vibration (1510 cm^{-1}), C–N stretching (1420 cm^{-1}), –CH$_2$– oscillation out of plane (1360 cm^{-1}), twisting vibration of –CH$_2$– (1250–1310 cm^{-1}), in-plane deformation

vibration of C–OH bond (1130 cm^{-1} and 1230 cm^{-1}), C–O stretching (1080–1130 cm^{-1}) and C–C stretching (1050 cm^{-1}) peaks [44]. By contrast, the FTIR of N-GQDs shows the intensification of O–H and N–H stretching, C–O stretching, deformation vibration of C–OH bond and C=O stretching, demonstrating that the oxygen content in the N-GQDs was increased, and that the number of oxygen-containing functional groups was also increased. Notably, the formation of C=C stretching (1650 cm^{-1}) and the intensification of −C−H stretching and C–C stretching peaks in N-GQDs, indicating that the formation of sp^2 (graphitic) or sp^3 (amorphous) carbon structures [45]. In addition, the distinct characteristic peak at 1220 cm^{-1} belongs to the stretching vibration of the C–O–C bond [46], it was presumably formed by decarboxylation of the CA as conjugating to GQDs. The presence of the N–H bond and the C–N bond on the N-GQDs also show L-Glu conjugated to the GQDs. Our fabrication method demonstrates that GQDs can be amino-functionalized during the synthesis process. Comparison to the two-step approach (first fabrication of GQDs, then amino-modification), the one-step method is easier and saves time. The amino-functionalized GQDs benefit from their biocompatibility; the groups of hydroxyl, carboxyl, carbonyl, and amino in the N-GQDs indicate its good hydrophilicity and stability in solution [47].

The XPS characterization was carried out in order to further analyze the elemental compositions and chemical bonds of the obtained N-GQDs. As illustrated in Figure 3A, the full scan spectrum of XPS exhibits three obvious peaks at 545.0, 402.2 and 298.1 eV, revealing the presence of O1s, N1s and C1s, respectively. Quantitative determination of the XPS spectrum shows that the as-prepared N-GQDs consisted of 36.42% O, 3.57% N and 60.01% C, indicating the successful doping of nitrogen into the GQDs. The C to O atomic ratio for the N-GQDs was about 1.65, which is slightly higher than that reported in [28] (1.51), demonstrating that the N-GQDs have a low oxidation level [48]. The N to C atomic ratio was calculated to be 0.06, which is as same as that reported in [28], but remarkably higher than that of the N-GQDs prepared using the electrochemical method (0.04) [49,50]. The deconvolution of the high-resolution XPS spectra of C1s (Figure 3B) reveals five main peaks, confirming the presence of C=C/C–C (284.5 eV), C–N (285.2 eV), C–OH (286.4 eV), C=O (287.3 eV), and O–C=O (288.9 eV) bonds [51], indicating that the as-prepared N-GQDs are rich in hydrophilic groups, such as hydroxyl, carboxyl, and carbonyl groups on the surfaces of N-GQDs, which is consistent with the result of FTIR. The deconvolution of the N1s spectrum (Figure 3C) shows three peaks at 399.9, 400.5, and 401.7 eV. The fitting results coincide well with the experimental results; the three peaks are attributed to the pyridinic N, pyrrolic N and graphitic N respectively [52], confirming again that nitrogen was partly doped into the GQDs. The fitted peaks at 532.1, 532.8 and 533.6 eV of O1s XPS spectrum shown in Figure 3D can be assigned to the three components C=O, C–O, and C–OH [53], respectively, which is in agreement with the XPS spectrum of C1s.
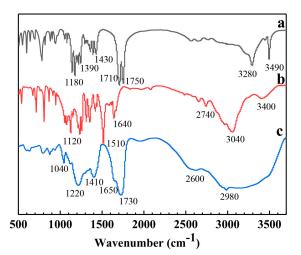

Figure 2. FTIR spectra of (**a**) CA, (**b**) L-Glutamic, and (**c**) N-GQDs.
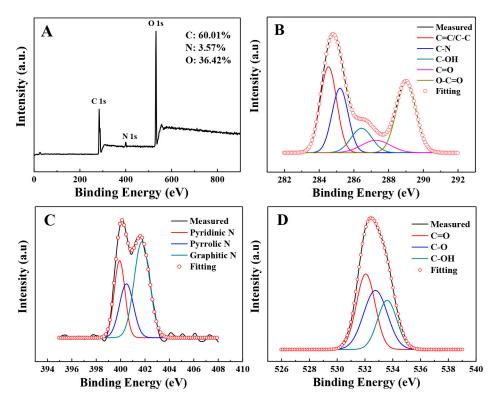
Figure 3. (**A**) Full scan XPS spectrum of the N-GQDs, and high solution XPS spectra of (**B**) C1s, (**C**) N1s, and (**D**) O1s.

3.3. Optical Properties

The UV-Vis absorption spectra (Figure 4A, Abs) of the N-GQDs aqueous solution shows an obvious absorption peak at 230 nm, which can be attributed to the $\pi \to \pi^*$ electronic transition of the aromatic sp^2 domains [54]; the absorption peak near 300 nm from the $n \to \pi^*$ transition of the heteroatom double bond in GQDs is very weak, indicating the existence of functional groups containing lone pairs of electrons (such as carboxyl groups, etc.) [55]; the excitation (Figure 4A, Ex) and emission (Figure 4A, Em) spectra exhibit good mirror symmetry; the N-GQDs emitted a very bright blue fluorescence that could be observed by naked eye (Figure 4A, inset). When the excitation wavelengths were changed from 300 nm to 500 nm (Figure 4B), the emission peaks of N-CQDs shifted from 430 nm to 548 nm (Figure 4C,D), and the maximum intensity was obtained at the excitation of 370 nm (Figure 4B); when the excitation was in the range of 300–370 nm, the emission peaks were almost invariable (~447 nm), indicating that the emission spectra are excitation independent; thus, from the emission was mainly produced by the carbon core (sp^2 domain) of the N-GQDs (band I) [56]. Meanwhile, with excitation in the range from 380 to 500 nm, the emission peaks increased with the excitation wavelength, implying that the emission originated from the transitions related to the surface states (hybridization of the carbon backbone and connected chemical groups) (band II). In [55], excitation-dependent emissions were associated with both the $n-\pi^*$ transition of the N/O surface groups and the $\pi-\pi^*$ charge transfer between the carbon core and the edge of the GQDs. The full width at half maximum (FWHM) of the strongest emission spectrum was only 87 nm. Compared with the reported GQDs synthesized with CA [57], our N-GQDs indicate a narrow emission range; the main reason for this is that L-Glu-functionalized GQDs decrease the surface defects. The QY of the N-GQDs was determined to be 54% (calculation data is shown in Table S1 of Supporting Information). This relatively high QY might be due to the low oxygen content [58], N doping and the protection of the L-Glu as the surface passivation agent. The high QY and narrow FWHM imply that the N-GQDs could be used for imaging or as fluorescent sensors.
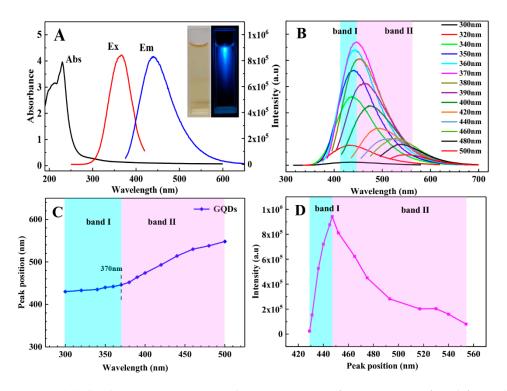
Figure 4. (**A**) The absorption, excitation and emission spectra of N-GQDs. Inset: from left to right are the N-GQDs aqueous solutions under ambient light and UV excitation (irradiated from an optical fiber), respectively; (**B**) the PL spectra of N-GQDs under excited different excitation wavelengths; (**C**) the peak positions and (**D**) the maximum intensities of the PL spectra varying with the excitation wavelengths in (**B**).

The photo-stability of the N-GQDs is easily influenced by photo-bleaching, pH value, temperature and preservation time. For practical applications, the photo-stability is very important. Here we probed this question in detail. The results show that the N-GQDs exhibited excellent photo-stability. Under continuous excitation (at 370 nm) for 50 min, the fluorescence intensity remained invariable, indicating the N-GQDs have superior photo-bleaching resistance (Figure 5A). Compared with previously reported N-GQDs [47,59], our N-GQDs show excellent photo-bleaching resistance. For comparison, the traditional organic dye Propidium iodide (PI) was also continuously irradiated for 50 min (Figure 5A, blue line); after irradiation for 10 min and 50 min, the intensity of PI decreased by 19% and 25%, respectively. The above results show that the prepared N-GQDs not only exhibit high QY, but also excellent photo-bleaching resistance. It can be inferred that the N-GQDs should be an excellent candidate for bioimaging.

The fluorescence intensities of the N-GQDs varying with pH value in the range of 2–9 (adjusted by HCl and NaOH) are shown in Figure 5B. Because the intensities did not show any obvious change with pH values in the range of 3–8, it was concluded that the as-prepared N-GQDs exhibit good stability under acid and neutral pH environments, and thus the protonation or deprotonation of the N-GQDs is also very weak [60–62]. Compared with the results reported in [63], the as-prepared N-GQDs can be used in a wide range of pH environments. Thus, the N-GQDs have good prospects for the fluorescence imaging of cells and other living organisms.
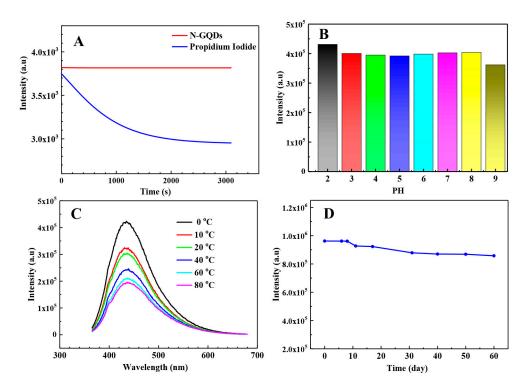
Figure 5. The photo-stability of the N-GQDs. (**A**) The photo-bleaching resistance of the N-GQDs and the traditional dye of propidium iodide; the PL peak intensities varying with (**B**) pH and (**C**) temperature; and (**D**) the PL peak intensities over 2 months.

The thermal stability of N-GQDS is also an important parameter for their application. The emission spectra of the N-GQDs were measured in the range of 0–80 °C. As shown in Figure 5C, the peak positions of the emission spectra were close to 447 nm, but the intensities decrease with increasing temperature, indicating that the thermal stability of the N-GQDS is not so good; the peak intensity at 40 °C is 80% of that at 20 °C.

Whether the N-GQDs can be preserved for a long time is also a significant index for their application. As shown in Figure 5D, the emission spectra of the N-GQDs were measured over a 60 d storage period. After storage at 4 °C for 8, 11, 17, 31, 40 and 60 days, the peak intensities at 447 nm of the emission spectra were 99.66%, 96.13%, 95.68%, 91.10%, 90.20% and 88.92% of the as-prepared N-GQDs, indicating that the N-GQDs can be stably preserved for at least 40 days.

The above results show that the ultrasonic hydrothermal approach is facile for obtaining N-doped GQDs with excellent photo-physical properties and stability.

3.4. Mechanism of Photoluminescence

To further investigate the emission mechanism of the N-GQDs, the fluorescence lifetime of the N-GQDs was measured using the time-correlated single photon counting (TCSPC) technique. The fluorescence lifetime of the N-GQDs was detected using an Edinburgh F900 time-resolved fluorescence spectrometer with an LED (370 nm). The monitor emission wavelength of the N-GQDs is 447 nm. The decay curve could be well fitted as a three-exponential function, and contains two fast decays (0.62 ns and 2.38 ns) and one slow decay (16.65 ns), which implies that the N-GQDs have two emission centers; the slow component lifetime is suggested to be related to the surface states in N-GQDs, while the quick lifetimes are related to the carbon core of the graphene structure in the N-GQDs [64]. The decay lifetimes are in good agreement with carbon-based quantum dots grown using different methods, such as chemical exfoliation [65] and the electrochemical method [66]. The average exciton lifetime (τ_{av}) is 2.653 ns. Additionally, the radiative (κ_r)

and nonradiative decay rate constants (κ_{nr}) can be obtained on the basis of the measured QY (φ) and average PL lifetime (τ_{av}) using the following equations [67]:

$$\kappa_r = \Phi/\tau_{av}. \tag{1}$$

$$\kappa_r + \kappa_{nr} = 1/\tau_{av} \tag{2}$$

The results are $\kappa_r = 2.04 \times 10^8 \text{ s}^{-1}$ and $\kappa_{nr} = 1.73 \times 10^8 \text{ s}^{-1}$.

Since both the source (CA and L-Glu) and the solvent (DI water) exhibit extremely weak UV absorption and emission, there should be a fluorescence emission originating from the N-GQDs. The fluorescence emission of the L-Glu-passivated N-GQDs can be attributed to the π electron transition of C=C in the core of N-GQD, which consists of a graphene structure and the surface groups of the N-GQDs [68]. As demonstrated above, our N-GQDs consist of a carbon core, as well as O-, H-, and N-containing functional groups on the surfaces of the N-GQDs. On the basis of the FTIR and XPS results, it can be seen that there are different kinds of functional groups (C-OH, C=O, C-O-C, C-H, C-N, and N-H) present on the surfaces of the N-GQDs; "surface states" are formed via the hybridization of the carbon backbone and the connected chemical groups, and the corresponding energy levels are situated between the π and π* states of sp^2 C [69]; therefore, the distributed surface states are a reasonable explanation for the difference in chemical bonding in the GQDs. The absorption and emission transitions of the N-GQDs and their energy levels are shown schematically in Figure 6C. In Figure 4C, the excitation-independent emission corresponds to excitation wavelengths of less than 370 nm; therefore, the energy difference between π and n can be estimated on the basis of the intrinsic excitation at 285 nm (4.35 eV) and 370 nm (3.35 eV) (Figure 6A), which is about 1.0 eV. The PL spectra from the carbon core of the graphene structure in the GQDs does not vary with excitation wavelength [56]; therefore, band I (in Figure 4B–D) is excitation independent. The surface states have various energy levels [70]; when a certain excitation wavelength illuminates the N-GQDs, a surface state emission dominates the emission; as the excitation wavelength changes, another corresponding surface state emission may become dominant. In addition to this, the electrons excited to π* may relax into surface states, emitting via radiative combination or not emitting via nonradiative combination. Thus, the excitation-dependent PL of the GQDs (band II in Figure 4B–D) is mainly a result of the surface states.

3.5. Fluorescence Cell Imaging with the N-GQDs

Most GQDs can be used for biomedical imaging because of their low cytotoxicity, excellent biocompatibility, high fluorescent QY, and excellent photo-bleaching resistance [71,72]. Herein, we used N-GQDs as fluorescent probes for the imaging of BV2 cells. Briefly, BV2 cells were placed on the confocal plate. The cells were cultured in Dulbecco's modified Eagle medium (DMEM) containing 1% penicillin–streptomycin and 10% fetal bovine serum (FBS) in an incubator with 5% CO_2 and 95% humidity at 37 °C. The culture solution was changed every other day. When the cell density reached about 80% (~5 × 10^4 cells/mL), 200 µg/mL N-GQDS was added to the cell medium and cultured at 37 °C and 5% CO_2 for 1 h. Finally, the BV2 cells were washed three times using PBS buffer (pH 7.4), and the morphology of the BV2 cells was observed and imaged using confocal LSM. The cells displayed enhanced blue (405 nm laser excitation) or green (488 nm laser excitation) fluorescence around their nucleus (Figure 7), indicating that the N-GQDs were able to label the cell membrane and the cytoplasm. Studies have shown that N-GQDs are likely to enter the cytoplasm, which can be attributed to the smaller amount of carboxyl on the surface of N-GQDs [68,73–76]. The abundant surface functional groups in N-GQDs (carboxyl, carbonyl, hydroxyl, and amino) ensure that they adhere easily to the negatively charged cell membrane [77–79], thus achieving effective uptake by cells. By comparing the bright field with the dark field images, the number of stained cells accounted for more than 90%, demonstrating the low cytotoxicity and good biocompatibility of the N-GQDs.
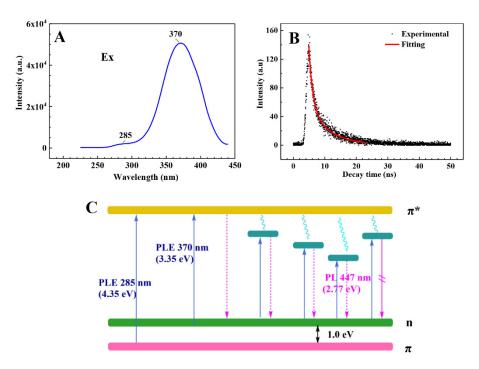
Figure 6. The photoluminescence mechanism of the N-GQDs: (**A**) the excitation spectrum obtained under the monitor emission wavelength at 447 nm and the excitation in the range of 200–430 nm; (**B**) the fluorescence lifetime of the N-GQDs; and (**C**) the schematic energy level of the N-GQDs.
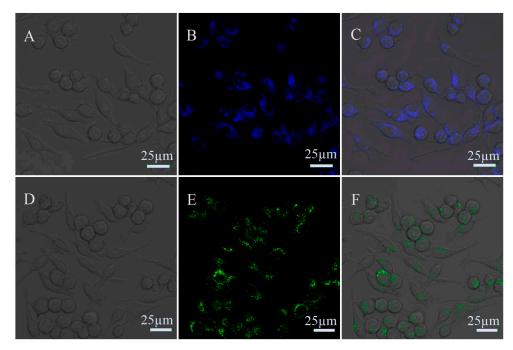

Figure 7. Laser scanning confocal fluorescence microscopy images of BV-2 cells: (**A,D**) the cells imaged under bright field, (**B**) 405 nm laser excitation, (**C**) overlay of (**A,B**), (**E**) 488 nm laser excitation, and (**F**) overlay of (**D,E**).

4. Conclusions

The ultrasonic-assisted hydrothermal method is a facile method for obtaining bright blue fluorescent N-doped GQDs with CA as a precursor and L-Glu for N doping. The morphology, size, structure, surface chemistry, optical properties, and stability subject to photo-bleaching, temperature, pH and preservation period of the N-GQDs were investigated in detail. The results showed that the N-GQDs possess sizes in the range of

3–6 nm, with an average size of 2.65 nm, containing 36.42% O, 3.57% N and 60.01% O, and possessing good water solubility, outstanding optical properties, excellent photo-bleaching resistance and stability, and good biocompatibility. The PL spectra of the N-GQDs are excitation dependent with excitation in the range of 300–370 nm and excitation independent with excitation in the range of 380–500 nm for core and surface state emissions. The QY reaches up to 54%. At room temperature and in the pH range of 3–8, the fluorescence of the N-GQDs is almost invariable. The N-GQDs can be stably preserved for at least 40 days. The average decay lifetime of the N-GQDs was measured to be 2.653 ns. The calculated radiative and nonradiative decay rate constants were 2.04×10^8 s^{-1} and 1.73×10^8 s^{-1}, respectively. The PL mechanism was explained qualitatively. The N-GQDs were used for BV2 cell imaging and showed good results, implying great potential applications for bioimaging or biomarking.

Supplementary Materials: The following are available online at https://www.mdpi.com/article/10.3390/nano11112798/s1, Figure S1: The absorption and PL spectra of N-GQDs obtained under different conditions, Table S1: Quantum yields of N-GQDs under different reaction conditions.

Author Contributions: H.W.: investigation, data curation, formal analysis, and writing—original draft; C.Q.: investigation and data curation; A.Y.: conceptualization, methodology, investigation, project administration, resources, supervision, writing and editing; X.W.: cell cultivation and cell imaging; J.X.: resources, cell cultivation and cell imaging. All authors have read and agreed to the published version of the manuscript.

Institutional Review Board Statement: Not applicable.

Informed Consent Statement: Not applicable.

Data Availability Statement: The data used to support the findings of this study are available from the corresponding author upon request.

Conflicts of Interest: The authors declare that they have no known competing financial interests or personal relationships that could have appeared to influence the work reported in this paper.

References

1. Geim, A.K.; Novoselov, K.S. The rise of graphene. *Nat. Mater.* **2009**, *6*, 11–19.
2. Liu, S.H.; Liu, Z.C.; Li, Q.F.; Xia, H.J.; Yang, W.J.; Wang, R.X.; Li, Y.X.; Zhao, H.; Tian, B.S. Facile synthesis of carbon dots from wheat straw for colorimetric and fluorescent detection of fluoride and cellular imaging. *Spectrochim. Acta A Mol. Biomol. Spectrosc.* **2021**, *246*, 118964. [CrossRef]
3. Liu, H.; Hao, C.; Nan, Z.; Qu, H.; Zhang, X.; Zhang, Z.; Sun, R. Fabrication of graphene oxide and sliver nanoparticle hybrids for fluorescence quenching of DNA labeled by methylene blue. *Spectrochim. Acta A Mol. Biomol. Spectrosc.* **2020**, *243*, 118802. [CrossRef]
4. Kuila, T.; Bose, S.; Mishra, A.K.; Khanra, P.; Kim, N.H.; Lee, J.H. Chemical functionalization of graphene and its applications. *Prog. Mater. Sci.* **2012**, *57*, 1061–1105. [CrossRef]
5. Tang, Q.; Zhen, Z. Graphene-analogous low-dimensional materials. *Prog. Mater. Sci.* **2013**, *58*, 1244–1315. [CrossRef]
6. Xu, J.; Qing, T.; Jiang, Z.; Zhang, P.; Feng, B. Graphene oxide-regulated low-background aptasensor for the "turn on" detection of tetracycline. *Spectrochim. Acta A Mol. Biomol. Spectrosc.* **2021**, *260*, 119898. [CrossRef] [PubMed]
7. Song, Y.; Qu, K.; Zhao, C.; Ren, J.; Qu, X. Graphene Oxide: Intrinsic Peroxidase Catalytic Activity and Its Application to Glucose Detection. *Adv. Mater.* **2010**, *22*, 2206–2210. [CrossRef] [PubMed]
8. Zheng, X.T.; Than, A.; Ananthanaraya, A.; Kim, D.H.; Chen, P. Graphene quantum dots as universal fluorophores and their use in revealing regulated trafficking of insulin receptors in adipocytes. *ACS Nano* **2013**, *7*, 6278–6286. [CrossRef] [PubMed]
9. Sun, H.; Wu, L.; Gao, N.; Ren, J.; Qu, X. Improvement of Photoluminescence of Graphene Quantum Dots with a Biocompatible Photochemical Reduction Pathway and Its Bioimaging Application. *ACS Appl. Mater. Interfaces* **2013**, *5*, 1174–1179. [CrossRef] [PubMed]
10. Kortel, M.; Mansuriya, B.D.; Vargas Santana, N.; Altintas, Z. Graphene Quantum Dots as Flourishing Nanomaterials for Bio-Imaging, Therapy Development, and Micro-Supercapacitors. *Micromachines* **2020**, *11*, 866. [CrossRef] [PubMed]

11. Wang, L.H.; Bu, Y.M.; Liu, Y.; Yao, Y.P.; Yang, Z.F.; Chen, P.; Tang, D.J.; Meng, L.; Cui, B. A Strategy for Microwave-Controlled Release of Anticancer Drugs: (Fe3O4/nGO) @mSiO2/GQDs Nanocomposite Carrier Jointly Enhanced by nGO and GQDs. *Nano* **2020**, *15*, 2050071. [CrossRef]

12. Li, R.; Cui, F.; Zhu, H.; Sun, X.; Li, Z. Electrochemical sensor for detection of cancer cell based on folic acid and octadecylamine-functionalized graphene aerogel microspheres. *Biosens. Bioelectron.* **2018**, *119*, 156–162.

13. Xu, H.; Zhou, S.; Xiao, L.; Wang, H.; Li, S.; Yuan, Q. Fabrication of a nitrogen-doped graphene quantum dot from MOF-derived porous carbon and its application for highly selective fluorescence detection of Fe3+. *J. Mater. Chem. C* **2015**, *3*, 291–297. [CrossRef]

14. Shehab, M.; Ebrahim, S.; Soliman, M.M. Graphene quantum dots prepared from glucose as optical sensor for glucose. *J. Lumin.* **2017**, *184*, 110–116. [CrossRef]

15. Pang, P.; Yan, F.; Li, H.; Li, H.; Zhang, Y.; Wang, H.; Wu, Z.; Yang, W. Graphene quantum dots and Nafion composite as an ultrasensitive electrochemical sensor for the detection of dopamine. *Anal. Methods* **2016**, *8*, 4912–4918. [CrossRef]

16. Ghosh, D.; Sarkar, K.; Devi, P.; Kim, K.H.; Kumar, P. Current and future perspectives of carbon and graphene quantum dots: From synthesis to strategy for building optoelectronic and energy devices. *Renew. Sust. Energ. Rev.* **2021**, *135*, 110391. [CrossRef]

17. Gupta, V.; Chaudhary, N.; Srivastava, R.; Sharma, G.D.; Bhardwaj, R.; Chand, S. Luminscent graphene quantum dots for organic photovoltaic devices. *J. Am. Chem. Soc.* **2011**, *133*, 9960–9963. [CrossRef] [PubMed]

18. Jin, Z.; Owour, P.; Lei, S.; Ge, L. Graphene, graphene quantum dots and their applications in optoelectronics. *Curr. Opin. Colloid. Interface Sci.* **2015**, *20*, 439–453. [CrossRef]

19. Son, D.I.; Kwon, B.W.; Park, D.H.; Seo, W.S.; Yi, Y.; Angadi, B.; Lee, C.L.; Choi, W.K. Emissive ZnO-graphene quantum dots for white-light-emitting diodes. *Nat. Nanotechnol.* **2012**, *7*, 465–471. [CrossRef]

20. Liu, J.; Liu, Y.; Liu, N.; Han, Y.; Zhang, X.; Huang, H.; Lifshitz, Y.; Lee, S.-T.; Zhong, J.; Kang, Z. Metal-free efficient photocatalyst for stable visible water splitting via a two-electron pathway. *Science* **2015**, *347*, 970–974. [CrossRef]

21. Yang, Z.; Xu, M.; Liu, Y.; He, F.; Gao, F.; Su, Y.; Wei, H.; Zhang, Y. Nitrogen-doped, carbon-rich, highly photoluminescent carbon dots from ammonium citrate. *Nanoscale* **2014**, *6*, 1890–1895. [CrossRef]

22. Pan, D.; Zhang, J.; Li, Z.; Wu, M. Hydrothermal route for cutting graphene sheets into blue-luminescent graphene quantum dots. *Adv. Mater.* **2010**, *22*, 734–738. [CrossRef]

23. Sangam, S.; Gupta, A.; Shakeel, A.; Bhattacharya, R.; Sharma, A.K.; Suhag, D.; Chakrabarti, S.; Garg, S.K.; Chattopadhyay, S.; Basu, B.; et al. Sustainable synthesis of single crystalline sulphur-doped graphene quantum dots for bioimaging and beyond. *Green Chem.* **2018**, *20*, 4245–4259. [CrossRef]

24. Dong, Y.; Shao, J.; Chen, C.; Li, H.; Wang, R.; Chi, Y.; Lin, X.; Chen, G. Blue luminescent graphene quantum dots and graphene oxide prepared by tuning the carbonization degree of citric acid. *Carbon* **2012**, *50*, 4738–4743. [CrossRef]

25. Kaewanan, P.; Sricharoen, P.; Limchoowong, N.; Sripakdee, T.; Nuengmatcha, P.; Chanthai, S. A fluorescence switching sensor based on graphene quantum dots decorated with Hg2+ and hydrolyzed thioacetamide for highly Ag+-sensitive and selective detection. *RSC Adv.* **2017**, *7*, 48058–48067. [CrossRef]

26. Du, F.; Jin, X.; Chen, J.; Hua, Y.; Cao, M.; Zhang, L.; Li, J.; Zhang, L.; Jin, J.; Wu, C.; et al. Nitrogen-doped carbon dots as multifunctional fluorescent probes. *J. Nanopar. Res.* **2014**, *16*, 2720. [CrossRef]

27. Chu, H.X.; Hu, J.; Li, R.; Yang, Y.Q. Electrochemical aptasensor for detection of acetamiprid in vegetables with graphene aerogel-glutamic acid functionalized graphene quantum dot/gold nanostars as redox probe with catalyst. *Sens. Actuators B Chem.* **2019**, *298*, 126866–126875.

28. Gavgani, J.N.; Dehsari, H.S.; Hasani, A.; Mahyari, M.; Shalamzari, E.K.; Salehi, A.; Taromi, F.A. A room temperature volatile organic compound sensor with enhanced performance, fast response and recovery based on N-doped graphene quantum dots and poly(3,4-ethylenedioxythiophene)–poly (styrene sulfonate) nanocomposite. *RSC Adv.* **2015**, *5*, 57559–57567. [CrossRef]

29. Liu, J.; Zhang, X.L.; Cong, Z.X.; Chen, Z.T.; Yang, H. Glutathione-functionalized graphene quantum dots as selective fluorescent probes for phosphate-containing metabolites. *Nanoscale* **2013**, *5*, 1810–1815. [CrossRef]

30. Zhu, S.; Zhang, J.; Liu, X.; Li, B.; Wang, X.; Tang, S.; Meng, Q.; Li, Y.; Shi, C.; Hu, R.; et al. Graphene quantum dots with controllable surface oxidation, tunable fluorescence and up-conversion emission. *RSC Adv.* **2012**, *2*, 2717–2720. [CrossRef]

31. Li, Y.; Zhao, Y.; Cheng, H.; Hu, Y.; Shi, G.; Dai, L.; Qu, L. Nitrogen-Doped Graphene Quantum Dots with Oxygen-Rich Functional Groups. *J. Am. Chem. Soc.* **2012**, *134*, 15–18. [CrossRef]

32. Qu, D.; Zheng, M.; Du, P.; Zhou, Y.; Zhang, L.; Li, D.; Tan, H.; Zhao, Z.; Xie, Z.; Sun, Z. Highly luminescent S, N co-doped graphene quantum dots with broad visible absorption bands for visible light photocatalysts. *Nanoscale* **2013**, *5*, 12272–12277. [CrossRef] [PubMed]

33. Ruiyi, L.; Tinling, P.; Hong-xia, C.; Jinsong, S.; Zaijun, L. Electrochemical detection of cancer cells in human blood using folic acid and glutamic acid-functionalized graphene quantum dot-palladium@gold as redox probe with excellent electrocatalytic activity and target recognition. *Sens. Actuators B Chem.* **2020**, *309*, 127709. [CrossRef]

34. Zhang, J.; Li, Y.; Han, S. Simultaneous detection of iodide and mercuric ions by nitrogen-sulfur co-doped graphene quantum dots based on flow injection turn off-on chemiluminescence analysis system. *Microchem. J.* **2019**, *147*, 1141–1146. [CrossRef]

35. Hatamluyi, B.; Rezayi, M.; Beheshti, H.R.; Boroushaki, M.T. Ultra-sensitive molecularly imprinted electrochemical sensor for patulin detection based on a novel assembling strategy using Au@Cu-MOF/N-GQDs. *Sens. Actuators B Chem.* **2020**, *318*, 128219. [CrossRef]

36. Oshima, C.; Nagashima, A. Ultra-thin epitaxial films of graphite and hexagonal boron nitride on solid surfaces. *J. Phys. Condens. Matter* **1997**, *9*, 1. [CrossRef]

37. Hong, G.; Zhao, H.-l.; Deng, H.; Yang, H.J.; Peng, H.; Liu, Y.; Chen, W. Fabrication of ultra-small monolayer graphene quantum dots by pyrolysis of trisodium citrate for fluorescent cell imaging. *Int. J. Nanomed.* **2018**, *13*, 4807–4815. [CrossRef]

38. Baskin, Y.; Meyer, L. Lattice Constants of Graphite at Low Temperatures. *Phys. Rev. Lett.* **1955**, *100*, 544. [CrossRef]

39. Novoselov, K.; Geim, A.K.; Morozov, S.; Jiang, D.; Zhang, Y.; Dubonos, S.; Grigorieva, I.; Firsov, A. Electric Field Effect in Atomically Thin Carbon Films. *Science* **2004**, *306*, 666–669. [CrossRef]

40. Peng, J.; Gao, W.; Gupta, B.K.; Liu, Z.; Romero-Aburto, R.; Ge, L.; Song, L.; Alemany, L.B.; Zhan, X.; Gao, G.; et al. Graphene Quantum Dots Derived from Carbon Fibers. *Nano Lett.* **2012**, *12*, 844–849. [CrossRef]

41. Tetsuka, H.; Asahi, R.; Nagoya, A.; Okamoto, K.; Tajima, I.; Ohta, R.; Okamoto, A. Optically tunable amino-functionalized graphene quantum dots. *Adv. Mater.* **2012**, *24*, 5333–5338. [CrossRef]

42. Tarakeshwar, P.; Manogaran, S. Ground state vibrations of citric acid and the citrate trianion—An ab initio study. *Spectrochim. Acta A Mol. Biomol. Spectrosc.* **1994**, *50*, 2327–2343. [CrossRef]

43. Gu, S.; Hsieh, C.-T.; Gandomi, Y.A.; Li, J.; Yue, X.X.; Chang, J.-K. Tailoring fluorescence emissions, quantum yields, and white light emitting from nitrogen-doped graphene and carbon nitride quantum dots. *Nanoscale* **2019**, *11*, 16553–16561. [CrossRef]

44. Jiang, Y.; Li, Y.; Li, Y.; Li, S. A sensitive enzyme-free hydrogen peroxide sensor based on a chitosan-graphene quantum dot/silver nanocube nanocomposite modified electrode. *Anal. Methods* **2016**, *8*, 2448–2455. [CrossRef]

45. Hou, X.B.; Li, Y.B.; Zhao, C. Microwave-Assisted Synthesis of Nitrogen-Doped Multi-Layer Graphene Quantum Dots with Oxygen-Rich Functional Groups. *Aust. J. Chem.* **2016**, *69*, 357–360. [CrossRef]

46. Zhang, T.P.; Wan, L.; Yuan, Y.; Duan, Y.X.; Zhang, J.M. Chemical Structure and Interlayer Distance Correlation of Graphite Oxide in the Heating Process as Revealed by In Situ Fourier Transform Infrared Spectroscopy and Wide-Angle X-ray Diffraction Techniques. *Appl. Spectrosc.* **2014**, *68*, 570–576. [CrossRef] [PubMed]

47. Wu, X.; Tian, F.; Wang, W.; Chen, J.; Wu, M.; Zhao, J.X. Fabrication of highly fluorescent graphene quantum dots using L-glutamic acid for in vitro/in vivo imaging and sensing. *J. Mater. Chem. C* **2013**, *1*, 4676–4684. [CrossRef] [PubMed]

48. Zhan, J.; Peng, R.; Wei, S.; Chen, J.; Peng, X.; Xiao, B. Ethanol-Precipitation-Assisted Highly Efficient Synthesis of Nitrogen-Doped Carbon Quantum Dots from Chitosan. *ACS Omega* **2019**, *4*, 22574–22580. [CrossRef] [PubMed]

49. Li, Y.; Hu, Y.; Zhao, Y.; Shi, G.; Deng, L.; Hou, Y.; Qu, L. An Electrochemical Avenue to Green-Luminescent Graphene Quantum Dots as Potential Electron-Acceptors for Photovoltaics. *Adv. Mater.* **2011**, *23*, 776–779. [CrossRef] [PubMed]

50. Shinde, D.; Vishal, V.M.; Kurungot, S.; Pillai, V. Electrochemical preparation of nitrogen-doped graphene quantum dots and their size-dependent electrocatalytic activity for oxygen reduction. *Bull. Mater. Sci.* **2015**, *38*, 435–442. [CrossRef]

51. Schroer, Z.S.; Wu, Y.; Xing, Y.; Wu, X.; Liu, X.; Wang, X.; Pino, O.G.; Zhou, C.; Combs, C.; Pu, Q.; et al. Nitrogen-Sulfur-Doped Graphene Quantum Dots with Metal Ion-Resistance for Bioimaging. *ACS Appl. Nano Mater.* **2019**, *2*, 6858–6865. [CrossRef]

52. Santiago, S.R.M.S.; Chang, C.-H.; Lin, T.N.; Yuan, C.T.; Shen, J.L. Diethylenetriamine-Doped Graphene Oxide Quantum Dots with Tunable Photoluminescence for Optoelectronic Applications. *ACS Appl. Nano Mater.* **2019**, *2*, 3925–3933. [CrossRef]

53. Li, H.J.; Sun, X.; Xue, F.; Ou, N.; Sun, B.-W.; Qian, D.J.; Chen, M.; Wang, D.; Yang, J.; Wang, X. Redox Induced Fluorescence On-Off Switching Based on Nitrogen Enriched Graphene Quantum Dots for Formaldehyde Detection and Bioimaging. *ACS Sustain. Chem. Eng.* **2018**, *6*, 1708–1716. [CrossRef]

54. Li, Y.; Liu, X.; Wang, J.; Liu, H.; Li, S.; Hou, Y.; Wan, W.; Xue, W.; Ma, N.; Zhang, J.Z. Chemical Nature of Redox-Controlled Photoluminescence of Graphene Quantum Dots by Post-Synthesis Treatment. *J. Phys. Chem. C* **2016**, *120*, 26004–26011. [CrossRef]

55. Li, L.; Wu, G.; Yang, G.; Peng, J.; Zhao, J.; Zhu, J.J. Focusing on luminescent graphene quantum dots: Current status and future perspectives. *Nanoscale* **2013**, *5*, 4015–4039. [CrossRef]

56. Yang, G.; Wu, C.; Luo, X.; Liu, X.; Gao, Y.; Wu, P.; Cai, C.; Saavedra, S.S. Exploring the Emissive States of Heteroatom-Doped Graphene Quantum Dots. *J. Phys. Chem. C* **2018**, *122*, 6483–6492. [CrossRef]

57. Bourlinos, A.B.; Stassinopoulos, A.; Anglos, D.; ZbpYil, R.; Karakassides, M.A.; Giannelis, E.P. Surface functionalized carbogenic quantum dots. *Small* **2008**, *4*, 455–458. [CrossRef]

58. Xu, X.; Gao, F.; Bai, X.; Liu, F.; Kong, W.; Li, M. Tuning the Photoluminescence of Graphene Quantum Dots by Photochemical Doping with Nitrogen. *Materials* **2017**, *10*, 1328. [CrossRef]

59. Kaur, M.; Kaur, M.; Sharma, V.K. Nitrogen-doped graphene and graphene quantum dots: A review onsynthesis and applications in energy, sensors and environment. *Adv. Colloid Interface Sci.* **2018**, *259*, 44–64. [CrossRef]

60. Moniruzzaman, M.; Kim, J. N-doped carbon dots with tunable emission for multifaceted application: Solvatochromism, moisture sensing, pH sensing, and solid state multicolor lighting. *Sens. Actuators B Chem.* **2019**, *295*, 12–21. [CrossRef]

61. Wu, Z.L.; Gao, M.X.; Wang, T.t.; Wan, X.Y.; Zheng, L.L.; Huang, C.Z. A general quantitative pH sensor developed with dicyandiamide N-doped high quantum yield graphene quantum dots. *Nanoscale* **2014**, *6*, 3868–3874. [CrossRef]

62. Vercelli, B.; Donnini, R.; Ghezzi, F.; Sansonetti, A.; Giovanella, U.; La Ferla, B. Nitrogen-doped carbon quantum dots obtained hydrothermally from citric acid and urea: The role of the specific nitrogen centers in their electrochemical and optical responses. *Electrochim. Acta* **2021**, *387*, 138557. [CrossRef]

63. Wang, R.; Du, X.; Wu, Y.; Zhai, J.; Xie, X. Graphene Quantum Dots Integrated in Ionophore-Based Fluorescent Nanosensors for Na^+ and K^+. *ACS Sens.* **2018**, *3*, 2408–2414. [CrossRef] [PubMed]

64. Choi, Y.; Kang, B.; Lee, J.; Kim, S.; Kim, G.T.; Kang, H.; Lee, B.R.; Kim, H.; Shim, S.H.; Lee, G.; et al. Integrative Approach toward Uncovering the Origin of Photoluminescence in Dual Heteroatom-Doped Carbon Nanodots. *Chem. Mater.* **2016**, *28*, 6840–6847. [CrossRef]
65. Zhu, X.; Zuo, X.; Hu, R.; Xiao, X.; Liang, Y.; Nan, J. Hydrothermal synthesis of two photoluminescent nitrogen-doped graphene quantum dots emitted green and khaki luminescence. *Mater. Chem. Phys.* **2014**, *147*, 963–967. [CrossRef]
66. Bao, L.; Zhang, Z.-L.; Tian, Z.Q.; Zhang, L.; Liu, C.; Lin, Y.; Qi, B.; Pang, D.W. Electrochemical Tuning of Luminescent Carbon Nanodots: From Preparation to Luminescence Mechanism. *Adv. Mater.* **2011**, *23*, 5801–5806. [CrossRef]
67. Dai, Y.; Long, H.; Wang, X.; Wang, Y.; Gu, Q.; Jiang, W.; Wang, Y.; Li, C.; Zeng, T.; Sun, Y.; et al. Doping: Versatile Graphene Quantum Dots with Tunable Nitrogen Doping. *Part. Part. Syst. Charact.* **2014**, *31*, 509. [CrossRef]
68. Liu, Q.; Guo, B.; Rao, Z.; Zhang, B.; Gong, J.R. Strong two-photon-induced fluorescence from photostable, biocompatible nitrogen-doped graphene quantum dots for cellular and deep-tissue imaging. *Nano Lett.* **2013**, *13*, 2436–2441. [CrossRef]
69. Qian, Z.; Ma, J.; Shan, X.; Shao, L.; Zhou, J.; Chen, J.; Feng, H. Surface functionalization of graphene quantum dots with small organic molecules from photoluminescence modulation to bioimaging applications: An experimental and theoretical investigation. *RSC Adv.* **2013**, *3*, 14571–14579. [CrossRef]
70. Zheng, X.T.; Ananthanarayanan, A.; Luo, K.Q.; Chen, P. Glowing Graphene Quantum Dots and Carbon Dots: Properties, Syntheses, and Biological Applications. *Small* **2015**, *11*, 1620–1636. [CrossRef]
71. Hu, C.F.; Liu, Y.L.; Yang, Y.H.; Cui, J.H.; Huang, Z.R.; Wang, Y.L.; Yang, L.F.; Wang, H.B.; Xiao, Y.; Rong, J.H. One-step preparation of nitrogen-doped graphene quantum dots from oxidized debris of graphene oxide. *J. Mater. Chem. B* **2013**, *1*, 39–42. [CrossRef]
72. Lin, L.; Rong, M.; Lu, S.; Song, X.; Zhong, Y.; Yan, J.; Wang, Y.; Chen, X. A facile synthesis of highly luminescent nitrogen-doped graphene quantum dots for the detection of 2,4,6-trinitrophenol in aqueous solution. *Nanoscale* **2015**, *7*, 1872–1878. [CrossRef]
73. Wang, Y.J.; Liu, Y.Q.; Gao, X.X.; Zhan, Y.S.; Pan, L.Y.; Zhang, W.K.; Fang, X.M. Surface Defect Passivation of Graphene Quantum Dots by Amino Functionalization and Photoluminescence Emission Enhancement. *Acta Phys. Chim. Sin.* **2016**, *32*, 2636–2644. [CrossRef]
74. Ju, J.; Zhang, R.; He, S.; Chen, W. Nitrogen-doped graphene quantum dots-based fluorescent probe for the sensitive turn-on detection of glutathione and its cellular imaging. *RSC Adv.* **2014**, *4*, 52583–52589. [CrossRef]
75. Du, Y.; Guo, S. Chemically doped fluorescent carbon and graphene quantum dots for bioimaging, sensor, catalytic and photoelectronic applications. *Nanoscale* **2016**, *8*, 2532–2543. [CrossRef]
76. Fan, Z.; Li, S.; Yuan, F.; Fan, L. Fluorescent graphene quantum dots for biosensing and bioimaging. *RSC Adv.* **2015**, *5*, 19773–19789. [CrossRef]
77. Lu, H.; Li, W.; Dong, H.; Wei, M. Graphene Quantum Dots for Optical Bioimaging. *Small* **2019**, *15*, 1902136. [CrossRef] [PubMed]
78. Younis, M.R.; He, G.; Lin, J.; Huang, P. Recent Advances on Graphene Quantum Dots for Bioimaging Applications. *Front. Chem.* **2020**, *8*, 424. [CrossRef] [PubMed]
79. Shin, Y.; Lee, J.; Yang, J.; Park, J.; Lee, K.; Kim, S.; Park, Y.; Lee, H. Mass production of graphene quantum dots by one-pot synthesis directly from graphite in high yield. *Small* **2014**, *10*, 866–870. [CrossRef]